Complex SAR phase history modeling using two dimensional parametric estimation techniques

Chinghui J. Ying, Hung-Chih Chiang, Randolph L. Moses, and Lee C. Potter

Department of Electrical Engineering, The Ohio State University, Columbus, OH 43210

ABSTRACT

Using a point scatterer assumption, high-frequency synthetic aperture radar (SAR) phase histories can be modeled as a sum of two-dimensional (2D) complex exponentials in additive noise. This paper summarizes our SAR signal modeling experience using the XPatch simulated scattering data. We apply several 2D parametric estimation techniques including 2D TLS-Prony, MEMP, 2D IQML, and 2D CLEAN to estimate the complex exponential model parameters. From the estimation results, we discuss the engineering trade-offs among memory requirement, computation requirement, and estimation accuracy.

Keywords: 2D exponential modeling, SAR imaging, performance evaluation.

1. INTRODUCTION

Over narrow viewing angles, high-frequency synthetic aperture radar (SAR) phase histories can be modeled as a sum of two-dimensional (2D) complex exponentials in additive noise.[1,2,3,4,5,6] The 2D exponential terms correspond to scattering centers on the object, and the exponential amplitude taper in angle and frequency accommodates anisotropic scattering behavior over frequency and angle. Scattering-center-based SAR modeling has application to feature-based automatic target recognition (ATR) (such as in the MSTAR program) and to data compression of SAR or ISAR imagery.[7] This paper summarizes our SAR signal modeling experience using the XPatch simulated scattering data.

Several authors have addressed the applicability of point scatterer models in real and/or simulated SAR complex phase modeling; others have also investigated the estimation accuracy of using parametric algorithms in SAR modeling. Sacchini *et al.*[3] developed 2D total least squares Prony techniques (2D TLS-Prony) for estimating scattering exponential parameters and successfully applied the algorithms to extract the electro-magnetic scattering features of a thin metal plate. Gupta[5] presented a 2D bandwidth extrapolation approach using the point scattering model and obtained radar images with improved resolution than the ones obtained using 2D inverse Fourier transform. Hua[4] showed that SAR (or ISAR) phase histories of moving objects can be well modeled by a sum of ideal point scatterers if both the radar bandwidth and the viewing angle region are relatively small. With this superimposed scatterers model, he developed a matrix pencil technique which successfully extracts closely clustered scatterers of a synthesized X-band stepped frequency ISAR data set.[4] In addition, Hua developed matrix enhancement and matrix pencil (MEMP) techniques[8] which can also be used to estimate the scattering parameters. Clark and Scharf[9] developed a 2D iterative quadratic maximum likelihood (2D IQML) algorithm to estimate 2D exponential model parameters, and the algorithm was used to model XPatch data.[10] De Graaf[2] developed a CLEAN-type algorithm, called the coherent deconvolution (CD) algorithm, and compared the performance of the developed CD technique with the previous CLEAN algorithm.[11]

While a number of exponential modeling techniques have been developed, relatively little work has appeared on comparisons of these algorithms to SAR phase history data. In this paper we apply the 2D TLS-Prony techniques, the MEMP techniques, the 2D IQML algorithm, and a 2D CLEAN variant to estimate the complex exponential model parameters. From the estimation results, we consider the engineering trade-offs among memory requirement, computation requirement, and estimation accuracy. Pepin *et al.*[10] presents a similar survey of related techniques; their conclusions differ from ours, mainly because the data used by Pepin *et al.* were pre-processed in an unusual way.

The paper is organized as follows. Section 2 presents the 2D exponential model used in our complex SAR modeling problem. In Section 3, we review several 2D exponential modeling techniques, including 2D TLS-Prony, MEMP, 2D IQML, and 2D CLEAN. In Section 4 we theoretically compare the memory and computation requirement of the algorithms. In addition, we apply the algorithms to XPatch synthetic data. Modeling errors are used for performance comparison. Section 5 summarizes the engineering tradeoffs and concludes our paper.

2. 2D EXPONENTIAL MODEL

Using the point scatterer assumption,[1,2,4,5,6,12] complex SAR phase histories can be modeled as a sum of exponential signals. For a 2D radar return, the 2D exponential signal model is given

$$y\,(m,\ n) = \sum_{i=1}^{q} a_i x_i^m y_i^n + e\,(m,\ n)\,, \quad m = 0, 1, \ldots, M-1, \ \ n = 0, 1, \ldots, N-1, \tag{1}$$

where $\{a_i\}_{i=1}^q$ are the amplitudes, $\{x_i,\ y_i\}_{i=1}^q$ are the 2D poles, and $e\,(m,\ n)$ is an additive complex white Gaussian noise with mean zero and variance $2\sigma^2$ (each of the real and imaginary parts of the noise has variance σ^2). We assume that $\{x_i,\ y_i\}_{i=1}^q$ are distinct, *i.e.*, $x_i \neq x_j$ or $y_i \neq y_j, \forall i \neq j$, $e\,(m,\ n)$ is uncorrelated with the signal components, and the real and imaginary parts of $e\,(m,\ n)$ are also uncorrelated. The indices m and n represent samples in frequency and angle, respectively.

Physically, the model describes a radar return as a sum of scatterers whose locations correspond to the angles of the 2D $\{x_i,\ y_i\}$ poles. The moduli of the poles ($|x_i|$ and $|y_i|$) model anisotropic frequency and angle behavior of the i^{th} scattering center, and the amplitudes model the intensities of the scattering responses. Although the model is simplified, it also reveals a great deal of geometrical information about radar responses.[13,12,14] In addition, for high frequency band radars (*e.g.*, X-Band radar), SAR phase histories for military targets often exhibit strongly localized scattering responses, which indicates that the undamped exponential model (*i.e.*, the pole moduli are one) is applicable. In this paper we will discuss both damped and undamped exponential models, depending on the estimation techniques under consideration.

Note that the exponential model in Equation (1) can be extended to model polarimetric data.[14] For different polarized radar transmitting signals, target scattering returns exhibit same pole information but different amplitude responses, *i.e.*, $\{x_i,\ y_i\}_{i=1}^q$ will be the same but $\{a_i\}_{i=1}^q$ will be different from each polarimetric channel. Instead of one 2D exponential sequence, multiple 2D exponential sequences can then be used to model multi-polarimetric returns in SAR applications.[14]

The problem we consider is to estimate the model parameters based on measurements. Formally, given a set of noisy measurements, $y(m,\ n)$, we want to estimate the model parameters, $\{a_i,\ x_i,\ y_i\}_{i=1}^q$. Under the normality assumption, the maximum likelihood estimator for this modeling problem is obtained by minimizing the sum of the squares error between the noisy measurements and the estimated data. However, the nonlinear and multimodal cost surface results in a difficult numerical optimization task. A variety of techniques have been suggested for suboptimal solutions to this problem; we briefly discuss several in the next section. It is our interest to understand how these suboptimal techniques perform in practice, especially in SAR imaging applications.

3. 2D ESTIMATION TECHNIQUES

3.1. 2D TLS-Prony Techniques

Sacchini *et al.*[3] proposed two TLS-Prony based 2D estimation algorithms based on decomposing the original 2D estimation problem into two one-dimensional (1D) estimation problems. To do so, first note that Equation (1) can be rewritten as

$$s\,(m,\ n) = \sum_{i=1}^{q} a_i y_i^n x_i^m = \sum_{k=1}^{K} \sum_{l=1}^{L_k} a_{k,l} y_{k,l}^n x_k^m = \sum_{k=1}^{K} c_k(n) x_k^m, \tag{2}$$

where

$$c_k(n) = \sum_{l=1}^{L_k} a_{k,l} y_{k,l}^n, \tag{3}$$

and where $q = \sum_{k=1}^{K} L_k$. This reparameterization enables the decomposition of the 2D estimation problem since the last term of Equation (2) is the 1D multi-snapshot exponential signal model. With this multi-snapshot exponential parameterization, one can use the 1D TLS-Prony algorithm[15,16] (or other pole estimation algorithms, such as Matrix Pencil[17] (MP), State Space techniques,[18] etc.) in conjunction with a least squares (LS) fit to estimate the x-poles, $\{x_k\}$, and the multi-snapshot amplitude coefficients, $c_k(n)$. After estimating $c_k(n)$, $y_{k,l}$ and $a_{k,l}$ can then be estimated using the same approach, but with "data" $c_k(n)$. We refer to this algorithm as 2D TLS-Prony1.

The estimates of the y-poles in the above algorithm can suffer from error propagation since the y-poles are estimated from estimate of $c_k(n)$. To eliminate this error propagation, Sacchini *et al.* proposed a second algorithm in which the above algorithm is used twice (the algorithm is referred as 2D TLS-Prony2). First, the algorithm is applied to estimate the x-poles and then the y-poles as above; second, it is employed to estimate the y-poles first, then the x-poles. A heuristic distance matching algorithm is used to match the x-poles from the first estimation process and the y-poles from the second one, thereby using the pole estimates with higher accuracy. Finally, the amplitude coefficients are computed by linear LS using the paired 2D poles.

The 2D TLS-Prony techniques are computationally efficient because they decompose the 2D estimation problem into 1D problems. However, the algorithms are sometimes difficult to use because we need to set an upper bound on L_k (*e.g.*, say there are at most L_k y-poles for each x-pole); after estimating all the parameters, the final model order can be determined using existing model order selection algorithms, such as AIC, MDL, or an energy threshold criterion. In addition, the pairing algorithm in 2D TLS-Prony2 is not robust for low SNR, as is demonstrated by simulations presented later.

3.2. MEMP Techniques

A matrix enhancement and matrix pencil (MEMP) approach was proposed by Hua[8] to estimate 2D poles. The approach uses the matrix pencil (MP) method (a generalized eigen-decomposition technique) to estimate the model parameters. The problem is then to identify a proper mechanism that the MP technique can be applied to. For no collocated poles (when no two poles have the same x coordinate or y coordinate), the original 2D data matrix can be used for this purpose.[19] However, the technique suffers from the rank deficiency problem for collocated poles. To address these problems, Hua[8] crafted a rank-enhanced data matrix by stacking windowed data sequences in a linear prediction fashion. With this rank-enhanced matrix, the MP method can be applied to estimate the 2D poles even for collocated pole cases, and an orthogonality-based pole pairing algorithm can be used.

Hua proposed two MEMP-based techniques. The first follows the principle described above (referred as MEMP1). The second assumes the noise covariance is known (we refer this second technique as MEMP2). By using prior noise covariance information, an MEMP-based technique using the covariance matrix of the enhanced data matrix is devised. The advantage of using this technique is to use the eigen-decomposition on the dimensionally-smaller covariance matrix instead of the SVD on the much larger enhanced data matrix, thereby saving both memory and computation.

The MEMP techniques have been shown to give accuracy near the Cramér-Rao bound for a simple test case of three exponential modes in white Gaussian noise.[8] In addition, they have the advantage over the 2D TLS-Prony techniques that they avoid rooting of high order polynomials. However, from our experience the MEMP techniques have two major drawbacks. First, their memory requirement is large due to the large rank-enhanced data matrix; this is especially true of MEMP1. Second, their performance is limited by deficiencies of the heuristic pole pairing algorithm; this problem seems to be more prevalent for higher model orders.

3.3. 2D IQML

The iterative quadratic maximum likelihood (IQML) method attempts to solve the nonlinear least squares minimization problem for the exponential model by using a prediction polynomial parameterization.[20,21] Clark and Scharf[9] developed a 2D extension of the original 1D IQML algorithm. Like IQML, the 2D IQML finds the poles as the roots of polynomials. The first polynomial gives the leading poles, and they are required to be distinct. These leading poles are then used in a Lagrange interpolating polynomial to find the second dimension poles. The Lagrange interpolating polynomial technique requires that the leading poles are distinct. In addition, the polynomial coefficients are estimated through an iterative multi-dimensional minimization procedure over an orthogonal subspace of high dimension.

Unlike other algorithms, the 2D IQML algorithm has no pairing problem since the pairing of the 2D poles is inherent in the algorithm. However, the convergence of the algorithm is not guaranteed and is sometimes very slow. In addition, the technique is memory intensive, even with sparse matrix implementation, because of the high dimension of the orthogonal subspace. The dimension of this space is $NM - q$ where NM is the number of total available data points and q is the model order; the algorithm uses large matrices, of size $(NM - q) \times (NM - q)$.

3.4. 2D CLEAN

The CLEAN algorithm is an FFT-based parametric estimation algorithm.[11,22] The algorithm uses the undamped exponential signal model and thus assumes ideal point scattering responses. Essentially the CLEAN algorithm recursively estimates complex undamped exponentials using 2D FFT. The algorithm first estimates the strongest undamped exponential signal from the frequency, amplitude and phase of strongest peak in the oversampled 2D FFT. This estimated strongest undamped exponential signal is then subtracted from the phase history. The above procedure is then repeated recursively until the residual error between the original phase history and the estimated phase history (constructed using the point scatterer parameter estimates) is below the known noise level.

Many variants of the above CLEAN algorithm have been developed in recent years. De Graaf[2,22] developed the so-called coherent deconvolution (CD) algorithm which refines the CLEAN estimates using an optimization procedure that minimizes the deconvolution residual. Pepin *et al.*[10] proposed a variant called the RELAX algorithm which recursively reestimates the parameters. Nevertheless, in this paper we will use the standard CLEAN algorithm with the following amplitude estimation modification. Instead of using the complex amplitudes of the peaks as the amplitude estimates, we estimate the complex amplitudes using the linear LS fit of the frequency estimates to the original SAR phase history. In addition, the complex amplitudes of previously estimated modes are re-estimated whenever a new mode is added. We also include an option to the stopping criterion in which the estimation process is terminated when the number of mode estimates reaches an upper bound. This prior information is used because it is often available in SAR applications; it may be available for specific target classes, or one may only be interested in the q highest energy modes on the target. We will refer this variant as the 2D CLEAN algorithm. We find that the 2D CLEAN algorithm is simple and computationally efficient. However, the algorithm is biased and is limited by the Fourier resolution.

4. COMPARISONS: MEMORY, COMPUTATION, AND PERFORMANCE

In this section we compare several aspects of the above algorithms in their ability to model SAR scattering data. The numerical, computational, and statistical properties of most of these algorithms have been analyzed in the literature; however, the results have not been widely compared, especially for problems and parameter settings relevant to SAR data. For example, asymptotic statistical properties are available for many of these algorithms, but in SAR signal processing the data length and SNR are rarely close to "asymptotically large". Also, we wanted to test the algorithms on realistic scattering data where neither the scattering signals nor the clutter fit the assumed signal or noise model. Finally, we are interested in cases where the number of scattering centers is significant (10-50), a case not often considered in the literature.

Three aspects of the algorithms are considered: memory requirement, computational load, and modeling accuracy.

Table 1: Memory bottlenecks of the 2D algorithms (in Bytes); L_x and L_y are the prediction orders; S_x and S_y are the oversampling factors.

Algorithm	Memory Bottleneck
2D TLS-Prony1&2	$N(M-L_x)\times(L_x+1)\times 16\times 6$
MEMP1	$L_xL_y\times(M-L_x+1)(N-L_y+1)\times 16\times 6$
MEMP2	$L_xL_y\times(M-L_x+1)(N-L_y+1)\times 16\times 2$
2D IQML	$(NM-q)^2\times 16\times 0.01\times 3$
2D CLEAN	$NM\times S_xS_y\times 16$

For memory requirement, we compare the memory bottlenecks from each estimation algorithm, *i.e.*, the most memory space required to perform the essential operation in each algorithm. For computational load, we will estimate the floating-point-operation (flop) counts for each algorithm; we sum the flop counts from the most demanding operations, which often account for 90% or more of the computation required for each algorithm.

To evaluate the modeling accuracy, we apply the algorithms to the XPatch data sets provided by ARPA. Because of the lack of the true signal scattering center parameters for the XPatch data, we use the weighted relative error (WRE) of the estimated SAR image as the evaluation criterion. Given noisy SAR phase history, $y(m,n)$, the WRE is defined as

$$\text{WRE} = \frac{\sum_{m=1}^{M}\sum_{n=1}^{N} w_{mn}|IFT\{y(m,n)-\hat{y}(m,n)\}|^2}{\sum_{m=1}^{M}\sum_{n=1}^{N} w_{mn}|IFT\{y(m,n)\}|^2}, \tag{4}$$

where $IFT\{\cdot\}$ is the inverse Fourier transform operation, $|\cdot|$ is the magnitude of a complex number, w_{mn} is the weighting for the (m,n) pixel, and $\hat{y}(m,n)$ is the estimated SAR phase history. Although different weighting functions can be used, in the simulations below we use the square root of the magnitudes of the original image, *i.e.*, $\sqrt{|IFT\{y(m,n)\}|}$. This weighting function emphasizes the high energy regions of the SAR image; these regions most likely contain the target of interest and good model accuracy is needed in this region for ATR and data compression applications.

4.1. Memory Requirement

To compare the memory requirement for the estimation algorithms used, we consider the most memory-demanding operation in each estimation algorithm. For example, the most memory-demanding operation for the 2D TLS-Prony techniques and MEMP1 is the SVD operation, for MEMP2 it is the autocorrelation matrix calculation, for 2D IQML it is the QR decomposition of the $NM-q$ dimensional orthogonal space, and for 2D CLEAN it is the oversampled 2D FFT operation. Table 1 summarizes the memory bottlenecks for the considered estimation algorithms. In the table we consider that the SAR phase histories are complex and each complex data point is represented in a double precision format (*i.e.*, 16 bytes are needed to represent a complex number). Also, L_x and L_y in the table are the prediction orders of the x-dimension and y-dimension, respectively; S_x and S_y are the oversampling factors in the x-dimension and y-dimension for the 2D CLEAN FFT computations; for 2D IQML, we assume that the orthogonal subspace is implemented using sparse matrix techniques, and with a matrix sparseness of 1%.

Using the entries in Table 1, we plot the memory requirement of the estimation algorithms versus the used SAR image size in Figure 1. We assume the images are square with size $N\times N$ pixels. For the linear prediction-based techniques (*i.e.*, the 2D TLS-Prony and MEMP techniques), the linear prediction orders are assumed to be $N/3$. For 2D IQML, we assume the model order is $N/4$. For 2D CLEAN, we assume that the oversampling factor is 4 for each dimension.

From Figure 1 we can see that the MEMP techniques require the most memory, and 2D CLEAN requires the least. In addition, the memory required in the MEMP techniques increases rapidly as the image size increases, and for even moderate size images, the memory demand is very large (*e.g.* more than 400 Mbytes for a 100×100 image).

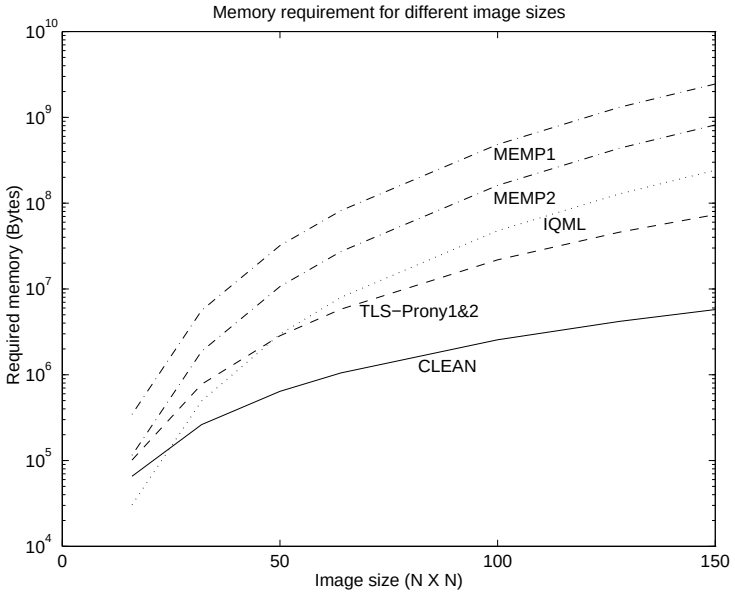

Figure 1: Different image size memory requirement using the 2D TLS-Prony techniques, the MEMP techniques, the 2D IQML technique, and the 2D CLEAN technique.

4.2. Computation Requirement

The computation bottlenecks of the algorithms include the following operations: SVD, QR, EVD, polynomial rooting, linear LS fitting, matrix inversion, 2D FFT, and peak finding. In Table 2, we summarize the flop counts[23] for these operations on a real-valued matrix of size $R \times C$. Since the tested SAR phase histories are complex, we also include approximate multiplicative factors for complex-valued matrices; we used **MATLAB** to estimate these factors. The total flop count for each operation is thus the product of the real matrix flops and the complex factor.

Table 2: Computation of various important operations

Operation	Flops for real matrix of $R \times C$	Approx. complex factor
Economy SVD	$14RC^2 + 8C^3$	2.5
Full SVD	$4R^2C + 8RC^2 + 9C^3$	2.5
Economy QR	$4C^2(R - C/3)$	4.0
Symmetric EVD	$9C^3$	8.5
Rooting	$10C^3$	4.0
Linear LS fitting	$2C^2(R - C/3)$	4.0
Inversion	$2C^3$	4.0
2D FFT	$RC\log_2(RC)$	10.5
Peak finding	$8RC$	4.0

In Table 3, we summarize the most computationally intensive operations for each estimation algorithm. Our simulation experiments show that the listed operations generally account for 90% or more of the total computation. For MEMP2, "Autocorrelation" means the computation required to calculate the large size autocorrelation matrix; for 2D IQML, "Iterations" means the number of iterations taken to obtain a convergent result; for 2D CLEAN, "Order Iterations" means the number of iterations taken to obtain all q modes, where q is the model order.

In Figure 2, we plot the computational loads of the considered algorithms versus the used SAR image size. We

Table 3: Computation bottlenecks of the 2D algorithms

Algorithm	Computation Bottleneck
2D TLS-Prony1&2	SVD, Rooting, LS fitting
MEMP1	QR, SVD
MEMP2	Autocorrelation, EVD
2D IQML	Iterations on (QR or LS fitting)
2D CLEAN	Order iterations on (2D IFFT, Peak Finding, LS fitting)

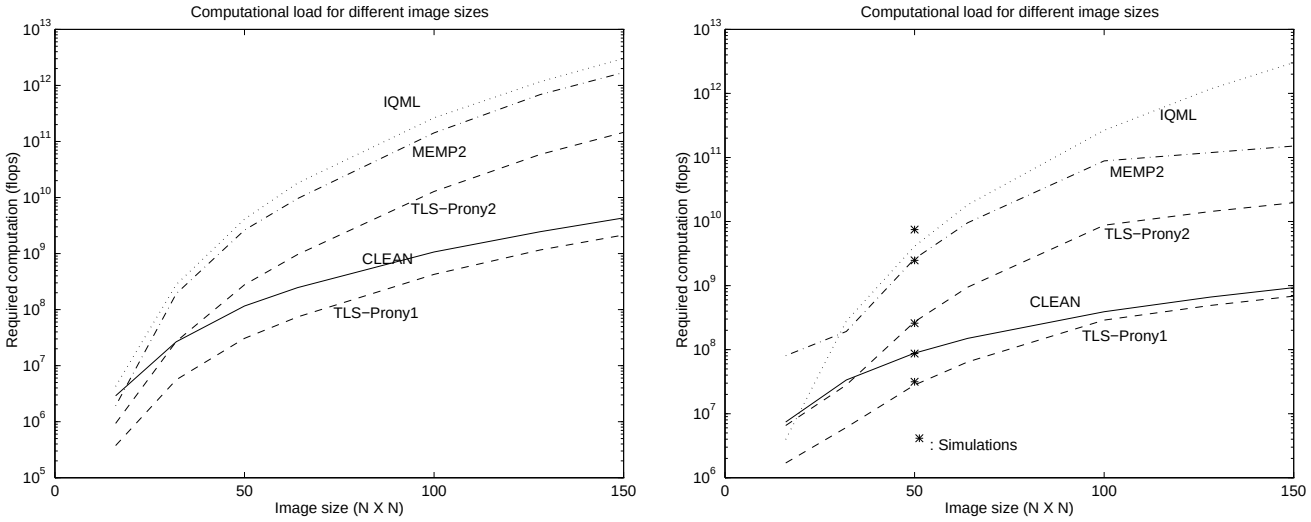

Figure 2: Different image size computational loads using the 2D TLS-Prony techniques, the MEMP techniques, the 2D IQML technique, and the 2D CLEAN; (a) varying model order as well as prediction order as a function of image size, (b) fixing model order $q = 10$ and prediction order L_x (or L_y) to be one-third of data length, but no less than 10 and no greater than 30.

consider two cases; in Figure 2(a) we vary the model order (order is $N/4$) and the prediction order ($N/3$) as a function of the image dimension, N, while in Figure 2(b) we fix the model order $q = 10$ and the prediction order to be one-third of the data dimension, but no less than 10 and no greater than 30. In addition, for 2D CLEAN we assume that the oversampling factor is 4; for 2D IQML we assume that 50 iterations are needed to obtain a convergent result, which tends to be a smaller figure than what we observe from the simulations.

It is clear from Figure 2 that 2D IQML requires the most computation. The 2D IQML computation prediction is conservative; in practice 2D IQML typically requires more computation because it often requires more than the 50 iterations we assumed for the computation prediction. 2D TLS-Prony1 requires the least computation. Also, we verify the theoretical prediction by using simulation whose results for corresponding algorithms are shown in Figure 2(b). The computational counts (shown by stars) are obtained by averaging 10 Monte-Carlo simulations using **MATLAB**. It is evident that the simulations and the theoretical results are in good agreement except for 2D IQML. The 2D IQML computation from simulation is higher than the one from the theory prediction; it is due to the fact that the average number of iterations used is about 70, instead of 50 used in the theoretical prediction. For larger N, the number of iterations needed for convergence can sometimes (far) exceed 100.

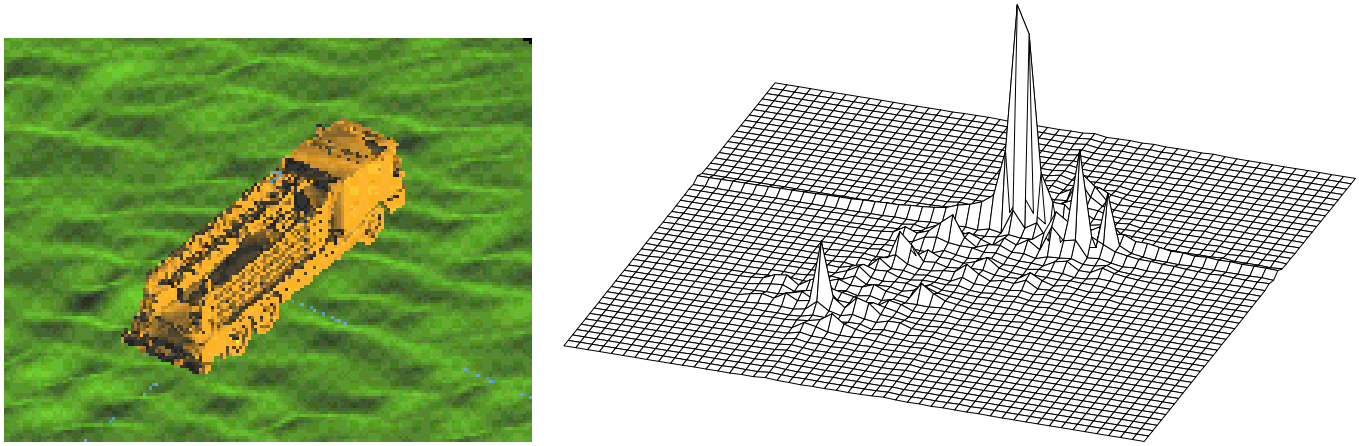

(a) (b)

Figure 3: (a) Fire truck CAD model used by XPatch, and (b) the corresponding SAR image.

4.3. Performance Evaluation Using XPatch Data

We apply the estimation algorithms to SAR phase history data of a fire truck on an uneven surface; the data were generated by XPatch. In Figure 3 we show the fire truck CAD model and one of the SAR images generated by XPatch from this CAD model. The center frequency used for the data set is 10 GHz, the bandwidth is 500 MHz, the elevation angle is 25°, HH polarization is used, and the SAR integration angle is 2.82°, resulting in an image resolution of 1 foot by 1 foot.

We tested the algorithms on four targets at azimuths from 0° to 360° in 2° degree increments. In general, the modeling results were good to excellent for azimuths away from cardinal angles, and fair to poor for azimuths near cardinal angles, with some variations in quality as a function of target. We present two typical results here, one at 54° azimuth representative of off-cardinal-angle performance, and one at 90° typical of the poor performance seen for targets on cardinal angles.

To increase the apparent clutter, we add complex white Gaussian noise to the synthetic XPatch SAR data. Different SNRs are used to evaluate the performance of the tested algorithms. In this paper, SNR is defined as

$$\text{SNR} = 10 \log_{10} \frac{P_s}{2\sigma^2}, \tag{5}$$

where $2\sigma^2$ is the total noise power, and P_s is the total signal power that is defined as

$$P_s = \frac{1}{NM} \sum_{m=1}^{M} \sum_{n=1}^{N} |s(m,n)|^2, \tag{6}$$

and $s(m,n)$ is the noiseless SAR phase history.

The experimental results are shown in Figures 4 and 5. We applied the exponential modeling algorithms to the fire truck phase histories at azimuth angles 54° and 90° (where 0° azimuth corresponds to nose-on). The phase histories used were 50-by-50, and 10 scattering centers were extracted from the data. Based on the extracted 10 scattering centers from each algorithm, the phase history was estimated using the 2D complex exponential model in Equation (1). The weighted relative error (WRE) is then calculated using this estimated phase history according to Equation (4). For all the algorithms except the 2D IQML technique, 10 Monte-Carlo simulations were run to calculate the averaged WREs; for the IQML curves, only 5 Monte-Carlo simulations were used to obtain the averaged WREs due to the high computational load of this method. The linear prediction orders for the TLS-Prony techniques and the MEMP techniques are 17 ($N/3$) for each dimension.

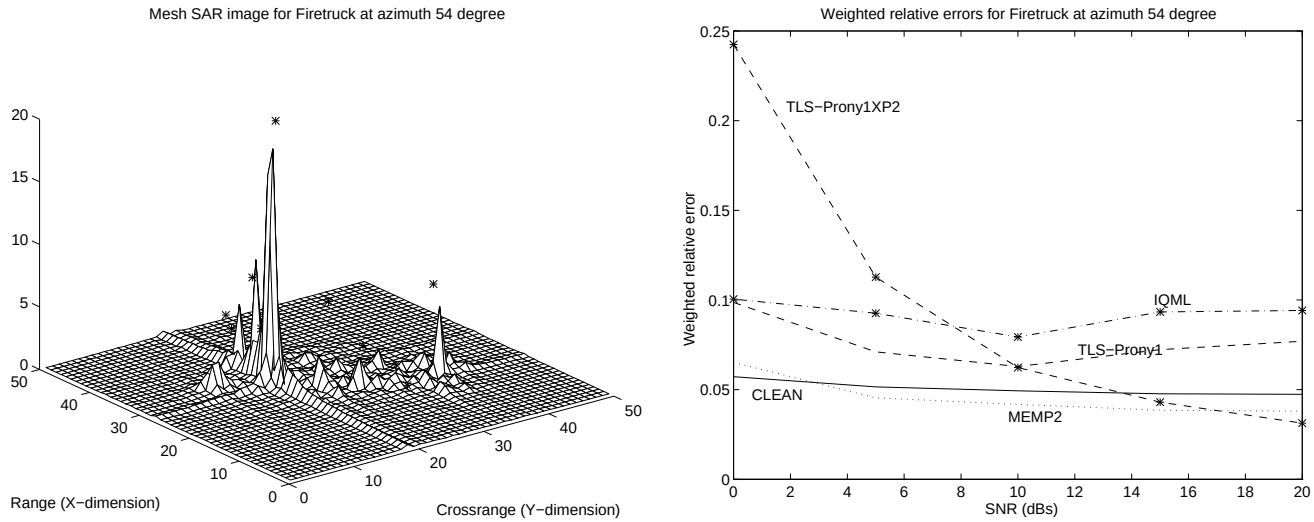

(a) (b)

Figure 4: (a) Estimated pole locations superimposed to the noiseless SAR image, and (b) the weighted relative error vs. SNR for fire truck at azimuth 54° .

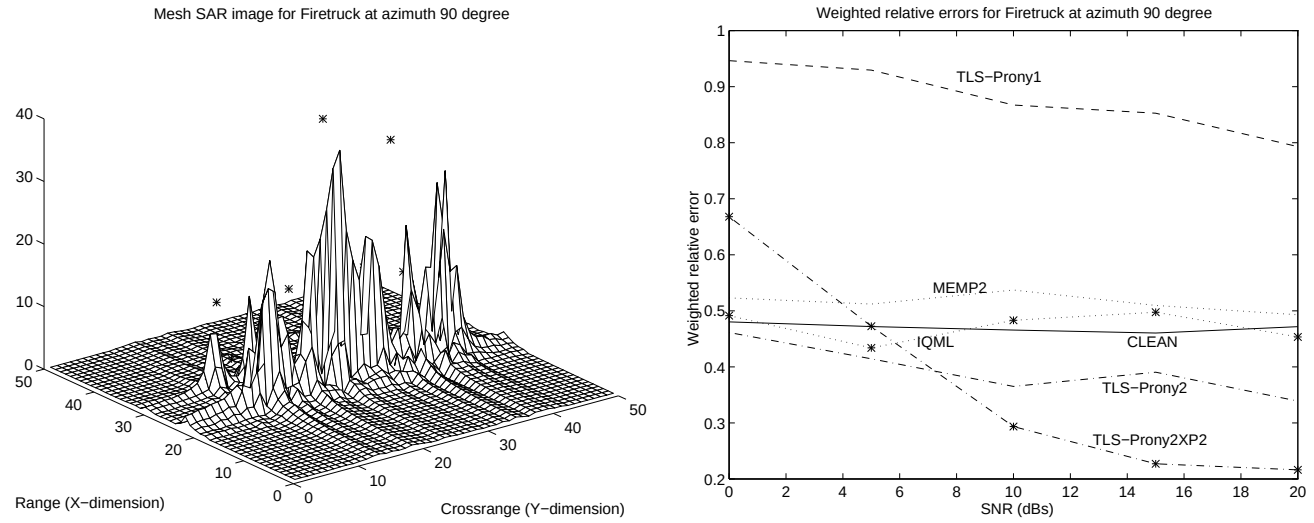

(a) (b)

Figure 5: (a) Estimated pole locations superimposed to the noiseless SAR image, and (b) the weighted relative error vs. SNR for fire truck at azimuth 90° .

Several conclusions can be drawn from the figures.

- In general, the estimation accuracy is good to excellent for the fire truck at azimuths away from cardinal angles (the WREs are less than 0.1 for most cases at 54°) but poor for the fire truck at cardinal angles. In addition, the techniques exhibit similar performance for the fire truck at azimuths away from cardinal angles (the WREs are generally within 5% of each other) but exhibit great differences for the fire truck at cardinal angles. This is probably because of the mismatch between the superimposed scatterers model and the broadside responses. For targets at broadside the scattering phenomenon in the phase history tends to be impulsive. The finite superimposed scatterers model in the image domain does not model impulsive behavior well, and the WREs are high for this case. On the other hand, the resulting model generally has one or more scattering centers at

the correct location of the impulsive scattering, even if the WRE fit error is large.

- The WRE curves are often fairly flat as a function of SNR, primarily because the WRE uses the noiseless image for the weighting function. As a result, errors due to noise and clutter are given low weight, and the WRE is not very sensitive to noise level. The curves tend to be dominated by model fit errors in the regions of strong scattering. Unweighted relative errors (not shown) show a decreasing error with increased SNR, as these errors are dominated by fit error in the "clutter" regions of the image.

- The 2D CLEAN algorithm tends to have good performance for the off-cardinal angles, and is relatively insensitive to noise. However, it inherits the resolution limitation of Fourier transforms, and produces biased results; the bias is not a dominant factor to the WREs in this case. It can be seen from Figures 4(b) and 5(b) that as SNR increases, the estimation performance of 2D CLEAN does not improve much and, most of all, is surpassed by non-FFT based parametric techniques.

- The 2D TLS Prony techniques often do not perform well, and need to be carefully tuned to achieve good performance. Their WRE performance is very sensitive to algorithm parameter settings, especially to the number of collocated poles (L_k in Equation (3)). This is illustrated in Figure 4(b), where we show two curves for 2D TLS-Prony1 (the performance for 2D TLS-Prony2 is similar). For the curve labeled with "TLS-Prony1XP2", we first chose 20 modes by choosing 2 y-poles for each x-pole, and we then chose the 10 highest energy modes as the estimates. This is in contrast to the curve labeled with "TLS-Prony1" in which we only chose 10 modes by choosing one y-pole for each x-pole. It can be seen that the performance for the more y-poles option is better for high SNRs and worse for low SNRs in comparison to the one from the one y-pole option. This is because the SAR image does exhibit more than one y-pole phenomenon (seen from Figure 4(a)) so that the more y-poles option generally should produce better results. However, this is only true for high SNRs since for low SNRs the variances of the estimates will be larger. The increased variances are due to the larger prediction orders (we used 33 instead of 17 since we need to choose 20 modes first).

- For the TLS-Prony techniques, the importance of pole collocation information is magnified in the broadside example (Figure 5), which has all the poles practically at the same x location*. It is seen from Figure 5(b) that 2D TLS-Prony1 literally fails, even with the two y-poles option (not shown here). However, the 2D TLS-Prony2 technique performs extremely well for this case. This is because the algorithm has the option to estimate 10 different y poles, which is well suited to this broadside example. Note that the 2D TLS-Prony techniques outperform the MEMP approach in most cases we show. This is mainly due to the poor pole pairing performance of the MEMP technique.

- For the MEMP techniques, we show results only for the MEMP2 algorithm because the memory requirement for MEMP1 exceeded the memory capacity of our workstations. It is seen from the figures that MEMP2 outperforms other techniques for the azimuth 54° case (except at the very high SNR) but performs less well for the broadside case. From our experience, this is mainly due to the suboptimal pole pairing algorithm. To improve the pole pairing algorithm, one can use exhaustive search techniques, but at very high computational cost.

- The performance and computation of the IQML approach depend on the tolerance used in terminating iterations. The smaller the tolerance, the better the estimation accuracy, but at a cost of more computations. The computational increase can be large for even modest increases in tolerance, and the algorithm can sometimes fail to converge when the tolerance is decreased.

The results in Figures 4 and 5, and the conclusions drawn from them, differ from those in a recent comparative paper by Pepin *et al.*[10]. One reason for the difference is that the data used by Pepin was later found to be zero padded, and the modeling approaches were applied to both the data and the zero padding. This resulted in larger relative errors than we see here.

*Although the poles are not at the very same location numerically, the closeness of the poles causes the numerical ill-condition so that the 2D TLS-Prony1 fails.

5. CONCLUSIONS

We considered the modeling of SAR phase history data for ATR and for data compression applications. We applied several 2D parametric estimation techniques including the 2D TLS-Prony techniques, the MEMP techniques, the 2D IQML algorithm, and the 2D CLEAN algorithm to estimate the SAR scattering feature parameters using the complex exponential models. From the estimation results, we considered the engineering trade-offs among memory requirement, computation requirement, and estimation accuracy.

We find that the 2D CLEAN algorithm requires the least memory and modest computation to extract the model parameters. The 2D CLEAN algorithm performance was fairly constant with respect to SNR for the weighted relative error on SAR data we considered. However, the 2D CLEAN algorithm is limited by the Fourier resolution and gives biased results; similar conclusions have been reached by De Graaf[22] and others.

Eigen-decomposition techniques, including the TLS-Prony methods and MEMP techniques, can give excellent performance but at significant computational cost. Performance degradation often comes from the pole pairing operation required in most of the methods.

The 2D IQML method can give very good estimation accuracy if properly initialized and if the convergence tolerance level is set low. However, the technique has very slow convergence rate, and hence has very high computational cost. If the tolerance is set higher to reduce computational cost (as was done in Figures 4 and 5), 2D IQML performance is similar to that of other methods which have lower computational cost.

Thus, FFT-based methods are robust but have limited performance; non-FFT techniques are often not robust and have high computational costs. This has led some authors to consider hybrid techniques that attempt to combine the advantages of both types of methods[2,10,24]. Hybrid techniques employ FFTs for robust initialization, and refine the model parameter estimates using optimization schemes. While hybrid techniques seem promising, they are not yet automated to the point that they are easily applicable to automatic SAR feature extraction.

Finally, we note that the performance of these modeling techniques vary significantly as a function of target aspect. This variation is often larger than the performance differences of the various algorithms we testes. For aspects near cardinal angles, the point scattering assumption embraced in these 2D models is not good, and significant errors between the data and its model are seen (although the estimated scattering centers are at the correct locations of the target scattering). For cardinal angles, models that more accurately represent non-point target scattering are needed to achieve more accurate data representation.

6. ACKNOWLEDGMENTS

This research was supported in part by the Advanced Research Project Agency under contract MDA972-93-1-0015 managed through Wright Laboratories.

7. REFERENCES

1. M. P. Hurst and R. Mittra, "Scattering center analysis via Prony's method," *IEEE Trans. Antennas and Propagation*, vol. AP-35, pp. 986–988, August 1987.
2. S. De Graaf, "Parametric estimation of complex 2-D sinusoids," in *IEEE Fouth Annual ASSP Workshop on Spectrum Estimation and Modeling*, pp. 391–396, August 1988.
3. J. J. Sacchini, W. M. Steedly, and R. L. Moses, "Two-dimensional Prony modeling and parameter estimation," *IEEE Transactions on Signal Processing*, vol. 41, pp. 3127–3137, November 1993.
4. Y. Hua, "High resolution imaging of continuously moving object using stepped frequency radar," *Signal Processing*, vol. 35, pp. 33–40, 1994.

5. I. J. Gupta, "High-resolution radar imaging using 2-D linear prediction," *IEEE Trans. Antennas and Propagation*, vol. AP-42, pp. 31–37, January 1994.

6. L. C. Potter, D.-M. Chiang, R. Carrière, and M. J. Gerry, "A GTD-based parametric model for radar scattering," *IEEE Transactions on Antennas and Propagation*, vol. 43, pp. 1058–1067, October 1995.

7. L.-C. T. Chang and W. D. Burnside, "A data compression and reconstruction technique for the scattered fields from complex targets," Tech. Rep. 727625-1, OSU, EE, ElectroScience Lab., January 1995.

8. Y. Hua, "Estimating two-dimensional frequencies by matrix enhancement and matrix pencil," *IEEE Transactions on Signal Processing*, vol. 40, pp. 2267–2280, September 1992.

9. M. P. Clark and L. L. Scharf, "Two-dimensional modal analysis based on maximum likelihood," *IEEE Transactions on Signal Processing*, vol. 42, pp. 1443–1452, June 1994.

10. M. P. Pepin, M. P. Clark, and J. Li, "On the applicability of 2-D damped exponential models to synthetic aperture radar," in *IEEE Proc. ICASSP 95*, (Detroit, MI), May 8-12 1995.

11. J. Tsao and B. D. Steinberg, "Reduction of sidelobe and speckle artifacts in microwave imaging: The CLEAN technique," *IEEE Trans. Antennas and Propagation*, vol. AP-36, pp. 543–556, April 1988.

12. L. C. Potter and R. L. Moses, "Attributed scattering centers for SAR ATR," *IEEE Trans. on Image Processing Special Issue on Automatic Target Detection and Recognition*, 1995. Submitted.

13. R. L. Dilsavor, *Detection of Target Scattering Centers in Terrain Clutter Using an Ultra-Wideband, Fully-Polarimetric Synthetic Aperture Radar.* PhD thesis, The Ohio State University, September 1993.

14. W. M. Steedly and R. L. Moses, "High resolution exponential modeling of fully polarized radar returns," *IEEE Transactions on Aerospace and Electronic Systems*, vol. AES-27, pp. 459–469, May 1991.

15. M. A. Rahman and K.-B. Yu, "Total least squares approach for frequency estimation using linear prediction," *IEEE Transactions on Acoustics, Speech, and Signal Processing*, vol. ASSP–35, pp. 1440–1454, October 1987.

16. R. Kumaresan and D. W. Tufts, "Estimating the parameters of exponentially damped sinusoids and pole-zero modeling in noise," *IEEE Trans. on ASSP*, vol. ASSP-30, pp. 833–840, December 1982.

17. Y. Hua and T. K. Sarkar, "Matrix pencil method for estimating parameters of exponentially damped/undamped sinusoids in noise," *IEEE Trans. on ASSP*, vol. ASSP-38, pp. 814–824, May 1990.

18. B. D. Rao and K. S. Arun, "Model based processing of signals: A state space approach," in *Proceedings of the IEEE*, vol. 80, pp. 283–309, February 1992.

19. S. Y. Kung, K. S. Arun, and D. B. Rao, "State-space and singular-value decomposition-based approximation methods for harmonic retrieval problem," *J. of Opt. Soc. of America*, vol. 73, pp. 1799–1811, December 1983.

20. Y. Bresler and A. Macovski, "Exact maximum likelihood parameter estimation of superimposed exponential signals in noise," *IEEE Trans. on ASSP*, vol. ASSP–34, pp. 1361–1375, October 1986.

21. R. Kumaresan, L. L. Scharf, and A. K. Shaw, "An algortihm for pole-zero modeling and analysis," *IEEE Trans. on ASSP*, vol. ASSP–34, pp. 637–640, June 1986.

22. S. De Graaf, "Coherent deconvolution II final report," tech. rep., Advanced Concepts Division, Optical Science Laboratory, ERIM, September 1990.

23. G. H. Golub and C. F. VanLoan, *Matrix Computations.* Baltimore, MD: Johns Hopkins, 2 ed., 1989.

24. C. J. Ying, S. C. Ahalt, and R. L. Moses, "Maximum likelihood estimation of exponential signals using artificial neural networks," in *in Proceedings of WCNN 93*, (Portland, Oregon), pp. VI–629–VI–632, July 11–15 1993.